NASA TECHNICAL NOTE

NASA TN D-5636

c. 1

EFFECTS OF PRESSURE DISTRIBUTIONS ON BLUFF TENSION-SHELL SHAPES

by James Wayne Sawyer

Langley Research Center
Langley Station, Hampton, Va.

NATIONAL AERONAUTICS AND SPACE ADMINISTRATION • WASHINGTON, D. C. • FEBRUARY 1970

1. Report No. NASA TN D-5636	2. Government Accession No.	3. Recipient's Catalog No.
4. Title and Subtitle EFFECTS OF PRESSURE DISTRIBUTIONS ON BLUFF TENSION-SHELL SHAPES		5. Report Date February 1970 6. Performing Organization Code
7. Author(s) James Wayne Sawyer		8. Performing Organization Report No. L-6743 10. Work Unit No. 124-07-23-05-23
9. Performing Organization Name and Address NASA Langley Research Center Hampton, Va. 23365		11. Contract or Grant No. 13. Type of Report and Period Covered Technical Note
12. Sponsoring Agency Name and Address National Aeronautics and Space Administration Washington, D.C. 20546		14. Sponsoring Agency Code

15. Supplementary Notes

A part of the information presented herein was included in a thesis entitled "Effects of Pressure Distributions on the Shape of Tension Shell Entry Vehicles" submitted in partial fulfillment of the requirements for the degree of Master of Science in Engineering Mechanics, Virginia Polytechnic Institute, Blacksburg, Virginia, May 1969.

16. Abstract

An investigation was conducted to improve the accuracy in calculating pressure distributions for various tension-shell decelerator shapes and to evaluate the effects on derived shapes resulting from the application of different pressure distributions. Pressure distributions given by Newtonian and integral-relation theory were each used to derive tension-shell shapes. Experimental pressure distributions were obtained from two wind-tunnel models – one model shape was derived by using a Newtonian pressure distribution and the other shape was derived by using an integral-relation pressure distribution for a Mach number of 3.0 – and were compared with theoretical pressure distributions. The tests were conducted at a Mach number of 3.0, at zero angle of attack, and at a Reynolds number of 10.4×10^6 based on maximum model diameter. Tension-shell shapes were also derived by using the experimental pressure distributions and were compared with both the Newtonian-derived shape and the integral-relation-derived shape for a Mach number of 3.0.

17. Key Words Suggested by Author(s)	18. Distribution Statement
Pressure distribution effects Bluff tension-shell shapes	Unclassified – Unlimited

19. Security Classif. (of this report)	20. Security Classif. (of this page)	21. No. of Pages	22. Price*
Unclassified	Unclassified	38	$3.00

*For sale by the Clearinghouse for Federal Scientific and Technical Information Springfield, Virginia 22151

EFFECTS OF PRESSURE DISTRIBUTIONS ON BLUFF TENSION-SHELL SHAPES*

By James Wayne Sawyer
Langley Research Center

SUMMARY

An investigation was conducted to improve the accuracy in calculating pressure distributions for various tension-shell decelerator shapes and to evaluate the effects on derived shapes resulting from the application of different pressure distributions. Pressure distributions given by Newtonian and integral-relation theory were each used to derive tension-shell shapes. Two pressure distribution models – one model shape was derived by using a Newtonian pressure distribution and the other shape was derived by using an integral-relation pressure distribution for a Mach number of 3.0 – were tested to obtain pressure distributions for comparison with theoretical pressure distributions. The tests were conducted at a Mach number of 3.0, at zero angle of attack, and at a Reynolds number of 10.4×10^6 based on maximum model diameter. Tension-shell shapes were also derived by using the experimental pressure distributions, and the resulting shapes were compared with both the integral-relation-derived shape for a Mach number of 3.0 and the Newtonian-derived shape. The results showed that the pressure distributions given by integral-relation theory were in good agreement with experimental pressure distributions, whereas the Newtonian pressures did not agree with experiment. Tension-shell shapes derived by using pressure distributions given by integral-relation theory were in excellent agreement with shapes derived by using experimental pressure distributions and were substantially shorter than shapes derived by using Newtonian pressure distributions. Although the pressure distributions predicted by integral-relation theory are somewhat dependent on nose radius and Mach number, the differences in the integral-relation-derived tension-shell shapes attributable to various nose radii and Mach number were much less than those noted between Newtonian- and integral-relation-derived tension-shell shapes.

---

*A part of the information presented herein was included in a thesis entitled "Effects of Pressure Distributions on the Shape of Tension Shell Entry Vehicles" submitted in partial fulfillment of the requirements for the degree of Master of Science in Engineering Mechanics, Virginia Polytechnic Institute, Blacksburg, Virginia, May 1969.

INTRODUCTION

Equations for determining the shape of a tension-shell decelerator (fig. 1) have been derived from linear-membrane theory by specifying a constant ratio of circumferential-stress to meridional-stress resultants; these equations are given in reference 1. The derived shape of the tension shell depends on the pressure distribution on the shell. Aerodynamic characteristics of shapes derived by assuming a pressure distribution given by Newtonian theory have been obtained over a wide range of Mach number, Reynolds number, and fineness ratio as reported in references 2 to 11. Pressure distributions given by Newtonian theory permit the equations of reference 1 to be integrated analytically, and Newtonian pressures have been used for designing tension shells for use at supersonic speeds. However, the validity of Newtonian theory for predicting tension-shell pressure distributions is open to question inasmuch as the experimental data of references 5 and 11 for long tension-shell shapes show poor agreement with Newtonian theory. Also, the experimental data of reference 12 for large-angle cones with proportions similar to those of bluff tension-shell shapes show that Newtonian theory does not describe the actual pressure distribution. This inadequacy of Newtonian theory and the lack of experimental pressure distributions on bluff tension-shell shapes pose the question of how the tension-shell shapes might have differed if they had been derived by using a more realistic pressure distribution.

A survey of the literature showed that pressures obtained from integral-relation theory are in good agreement with experimental pressures obtained from tests on large-angle cones. (See ref. 12.) Integral-relation theory, however, does not permit analytical integration of the shape equations; consequently, a computational method has been developed for deriving bluff tension-shell shapes by use of an iteration procedure. In order to verify the pressure distribution obtained from this method, pressure distributions were determined from wind-tunnel tests conducted at a Mach number of 3.0 on two models, one with a shape that was derived from Newtonian pressure distributions and the other with a shape derived from integral-relation pressure distributions.

The present report compares the shapes derived from the theoretical and the experimental pressure distributions; it also compares the experimental pressure distributions with those assumed in the shape derivation. Inasmuch as the pressure distributions given by the integral-relation method are dependent on Mach number and the size of the spherical nose cap (fig. 1), the effects on the derived shapes of varying the Mach number from 2.5 to 7.0 and of varying the nose radius from 0.05 to 0.56 times the base radius are also discussed.

SYMBOLS

The units used for the physical quantities defined are given in the International System of Units (SI). (See ref. 13.)

A	projected area
A_b	projected base area, πr_b^2
a^*	sonic velocity, nondimensionalized by free-stream velocity
C_D	drag coefficient, $\frac{\int C_p dA}{A_b}$
C_p	pressure coefficient, $p - p_\infty$
d	maximum model diameter
K	body surface curvature, nondimensionalized by r_b
M	Mach number
N_0	N_φ evaluated at $r = r_b$
N_α, N_φ	circumferential- and meridional-stress resultants, respectively, positive in tension (see fig. 2)
P	nondimensional membrane pressure differential, $p - p_b$
p	local surface pressure, nondimensionalized by q_∞
p_b	base pressure, nondimensionalized by q_∞
p_∞	free-stream static pressure, nondimensionalized by q_∞
q_∞	free-stream dynamic pressure
R	nondimensional model coordinates, $\frac{r}{r_b}$

ΔR integration step size

r_b base radius (see fig. 2)

r_n model nose radius (see fig. 3)

s,n curvilinear coordinates along body surface, nondimensionalized by r_b (see fig. 3)

s^* sonic point on model surface

u,v velocity components in s and n direction, respectively, nondimensionalized by free-stream velocity

X nondimensional model coordinate, $\frac{x}{r_b}$

x,r model coordinates (see fig. 2)

Z tension-shell shape parameter, $\frac{q_\infty r_b}{N_0}$

$\alpha = \frac{N_\alpha}{N_\varphi}$

β shock angle (see fig. 3)

γ ratio of specific heats

δ shock-layer thickness along n-coordinate, nondimensionalized by r_b (see fig. 3)

θ surface angle, $\frac{\pi}{2} - \varphi$

$\lambda = \beta - \theta$

ρ density, nondimensionalized by ρ_∞

τ combined entropy-continuity flow variable, $\left(\frac{p}{\rho\Phi}\right)^{\frac{1}{\gamma-1}}$

Φ stagnation streamline isentropic constant, $\frac{p_1(0)}{\left(\rho_1(0)\right)^\gamma}$

φ meridional coordinate (see fig. 2)

Subscripts:

0 quantities along surface (n = 0)

1 quantities along shock wave (n = δ)

∞ free-stream conditions

SHAPE DETERMINATION

Statement of Problem

The problem of shape determination involves the solution of two sets of differential equations with their respective boundary conditions. The first set of equations, derived in reference 1, comes from the linear-membrane equilibrium equations for a shell of revolution subjected to an axisymmetric pressure distribution. The ratio of circumferential-stress to meridional-stress resultants is considered to be a constant, and zero axial forces are assumed on the compression ring. (See fig. 1.) The second set of equations is obtained from reference 12 by applying one-strip integral-relation theory to the solution of supersonic, inviscid flow around bluff bodies. The body surface is assumed to be normal to the free-stream flow direction at the nose, and the local velocity is assumed to be sonic at the sharp corner on the base compression ring. The two sets of equations are related in that the first set of equations requires a pressure distribution as an input in order to provide a shape and the second set of equation requires a shape as an input in order to provide a pressure distribution. An iterative procedure is used in which either a particular shape or a particular pressure distribution must be assumed before the calculations are begun, and the inputs to the two sets of equations are alternated until a unique shape and a unique pressure distribution are obtained.

Basic Equations and Solutions

Structural.- For a shell of revolution subject to an axisymmetric pressure distribution, reference 1 gives the appropriate linear-membrane equilibrium equations. In the notation of the current paper, the equations are as follows:

$$\frac{d\varphi}{dR} + \frac{\alpha}{R} \tan \varphi - \frac{ZP}{\cos \varphi} (R)^{1-\alpha} = 0 \qquad (1)$$

and

$$\frac{dX}{dR} = -\tan \varphi \tag{2}$$

with boundary conditions,

$$\tan \varphi = 0 \qquad (R = 1) \tag{3}$$

and

$$X = 0 \qquad (R = 1) \tag{4}$$

where $\alpha = \frac{N_\alpha}{N_\varphi}$ has been chosen as a constant, P is the nondimensional pressure differential across membrane, $R = \frac{r}{r_b}$, and $Z = \frac{q_\infty r_b}{N_0}$. Thus, for any particular pressure distribution, there exists a first-order differential equation (eq. (1)) and the necessary boundary condition (eq. (3)) to solve for the model surface slope. Equation (2), subject to the boundary condition (eq. (4)), may be integrated with respect to R to obtain the X-coordinate of the desired configuration as a function of R.

Equations (1) and (2), subject to the boundary conditions (eqs. (3) and (4)), have been solved for a body of revolution with an axisymmetric pressure distribution by the use of a digital computer. A source program in Fortran IV language is given in the appendix. Equations (1) and (2) were numerically integrated by use of the forth-order Runge-Kutta integration technique. The integration was started at $R = 1$ and continued with decreasing values to $R = 0$. In order to use the program, values of Z, α, ΔR, and a pressure distribution as a function of R are necessary inputs to the program. The program output consists of values of the axial coordinate x and surface slope φ as a function of R. With this program, shapes are obtained with zero nose radius of curvature.

Aerodynamic.- For a blunt body of revolution with sharp corners subjected to inviscid supersonic flow, the governing differential equations for the one-strip integral-relation method (ref. 12) may be written as follows:

$$\frac{d\delta}{ds} = (1 + K\delta) \tan \lambda \tag{5}$$

$$\frac{d\beta}{ds} = \left[(1 + K\delta)\left(\tan \lambda - \frac{\delta \sin \theta}{r_0}\right)\rho_1 u_1 v_1 - (2 + K\delta)\frac{r_1}{r_0}\rho_1 v_1^2 + K\delta \rho_0 u_0^2 + 2\left(1 + K\delta + \frac{r_1}{r_0}\right)(p_0 - p_1)\right]\left(\delta \frac{r_1}{r_0} \frac{\partial \rho_1 u_1 v_1}{\partial \beta}\right)^{-1} \tag{6}$$

and

$$\frac{du_0}{ds} = \left\{ \left(\tau_1 u_1 - \tau_0 u_0\right)\frac{d\delta}{ds} - \frac{\delta \sin\theta}{r_0}\left[\tau_0 u_0 + (1 + K\delta)\tau_1 u_1\right] - \frac{r_1}{r_0}\left[\delta\frac{\partial}{\partial\theta}\left(\tau_1 u_1\right)\frac{d\beta}{ds} + (2 + K\delta)\tau_1 v_1\right]\right\}\left[\delta\tau_0\left(1 - M_0^2\right)\right]^{-1} \tag{7}$$

The parameters in these equations are nondimensional and are described in the list of symbols. A sketch of the geometry and coordinates is shown in figure 3. A particular body contour is specified by giving the surface angle θ and curvature K as a function of s. On the axis of symmetry at $s = 0$, the body surface must be normal to the stream direction ($\varphi(0) = 0$) and the surface slope must be continuous; thus, the following conditions hold:

$$\beta(0) = \frac{\pi}{2} \tag{8}$$

and

$$u(0) = 0 \tag{9}$$

The surface speed is required to reach sonic velocity at the model corner $R = 1$, which results in the boundary condition

$$u_0(s^*) = a^* \tag{10}$$

where a^* is a constant dependent on M_∞ and γ.

Thus, three interconnected first-order differential equations (eqs. (5), (6), and (7)) and three boundary conditions (eqs. (8), (9), and (10)) must be satisfied. The functions at the shock wave are explicit functions of γ, M_∞, β, and θ. The main dependent variables are δ, β, and u_0; p_0 and ρ_0 are obtained as explicit functions of γ, M_∞, and u_0 by using the isentropic law.

Equations (5), (6), and (7) and the boundary conditions (8), (9), and (10) have been programed for use on a digital computer. The integration of equations (5), (6), and (7) starts at $s = 0$ and terminates at $s = s^*$; the initial shock-wave standoff distance $\delta(0)$ is unknown and must be chosen so that equation (10) is satisfied. A discussion of the techniques used in solving the equations and a detailed program listing are given in reference 12 with sample calculations for four blunt axisymmetric bodies.

To use the program of reference 12 to calculate the pressure distributions on the bluff tension-shell shapes of this study, the input statements and the shape subroutine of the program were modified so that the program would accept tabulated body shapes. With these modifications, flow conditions may be computed for any bluff body for which the surface slope is continuous and given as a function of r.

Calculation Procedure

To begin the iterative procedure involving equations (1) to (10), either a shape or a pressure distribution must be assumed. An initial shape was calculated by using a Newtonian pressure distribution $\left(\text{i.e., } P = C_{p,0} = 2 \sin^2\theta\right)$, and this shape was used in the integral-relation computer program involving equations (5) to (10) to obtain a new pressure distribution. To satisfy the requirements of the integral-relation computer program that the surface slopes be continuous and that the body surface be normal to the stream direction at the nose, the initial shape was given a spherical nose radius. The resulting pressure distribution was used in the linear-membrane program involving equations (1) to (4) which calculated a new shape that had a zero nose radius of curvature. The new shape was spherically blunted, and the procedure was repeated until convergence occurred to give a unique shape and pressure distribution. The process was considered to have converged if the difference between successive iterations resulted in a maximum variation in x/r_b of less than 0.0001.

APPARATUS AND TESTS

Models and Instrumentation

Two pressure distribution models were tested in a wind tunnel as part of the current investigation. The shapes and pertinent model dimensions are given in figure 4; model coordinates and orifice locations are given in table I. The model shapes were derived by using values of $Z = 0.65$ and $\alpha = 0$. For one of the shapes, a Newtonian pressure distribution was assumed; for the other shape, a pressure distribution predicted by integral-relation theory at a Mach number of 3 was used. Both shapes had a ratio of nose radius to base radius r_n/r_b of 0.20. Each model was instrumented with 49 pressure orifices; 41 orifices were distributed along the front face of the model, and 8 orifices were distributed along the model base region. The orifices along the front face of the models were positioned along two meridians 180° apart and were mounted flush with, and normal to, the model surface. The base pressures were measured at the open ends of tubes soldered along the model base. (See fig. 5.) The models were machined from mild steel, and the surfaces were polished to a smooth, bright finish.

Surface pressures were measured on each of the configurations by means of pressure transducers that were connected to the orifices by approximately 8 meters of steel tubing which had an inside diameter of 0.229 centimeter. In addition to the surface-pressure orifices, four total-pressure probes and four total-temperature probes were mounted on the walls of the tunnel to monitor the free-stream flow conditions. Transducers with accuracies of ± 1 percent of the maximum pressure range were used for all pressure measurements. Care was exercised in choosing transducers which had a

maximum range that matched the pressures to be measured as closely as possible. The output from all the pressure transducers and the thermocouples was recorded by the Langley central data recording facility.

Test Facility

All tests were conducted in the Langley 9- by 6-foot thermal structures tunnel. (See ref. 14.) This facility is a supersonic blowdown wind tunnel which operates at a Mach number of 3.0 at stagnation pressures from 345 to 1380 kN/m^2 and at stagnation temperatures from ambient to 1388 K. The air storage capacity is sufficient to permit tests of 2 minutes duration for stagnation pressures of 345 kN/m^2. The models were sting mounted as shown in figure 6 and were alined at zero angle of attack.

Test Procedure

All tests were conducted at a stagnation temperature of 395 K and at a stagnation pressure of 414 kN/m^2. The corresponding Reynolds number, based on the maximum body diameter, was approximately 10.4×10^6. Constant flow conditions were maintained for approximately 40 seconds to insure that all pressures had stabilized. Two tests were made on each model to evaluate pressure data and to determine the experimental accuracies. For the second test, the pressure transducers were interchanged.

RESULTS AND DISCUSSION

Analytical

Comparison of Newtonian and integral-relation pressure distributions and corresponding tension-shell shapes.- Tension-shell-shape coordinates that were computed by using Newtonian pressure distributions and the corresponding coordinates that were obtained from the iteration procedure by using integral-relation theory are presented in table II. For the present study, three Newtonian-derived tension-shell shapes with values of the shape parameter Z of 0.50, 0.65, and 0.80 and of $\alpha = 0$ were used as initial shapes in the iteration procedure. As the shape parameter was increased, the body length increased. Consequently, these values of Z were chosen to yield shapes that were sufficiently bluff to generate a detached bow shock wave and to permit the use of the integral-relation theory. For these shapes, $r_n = 0.05r_b$ was used in the integral-relation computer program to obtain the pressure distributions. Table II also includes the shape coordinates that resulted from the studies of the effects of nose radius and Mach number on tension-shell shapes derived from integral-relation theory. In both studies, the shape for $Z = 0.65$ was used. For the study of nose radius effects, shapes were computed for nose radii of $r_n = 0.05r_b$, $0.20r_b$, and $0.56r_b$ and for $M_\infty = 3.0$.

For the study of Mach number effects, shapes with $r_n = 0.05r_b$ were computed for Mach numbers of 2.5, 3.0, 5.0, and 7.0. Corresponding pressure distributions and drag coefficients predicted by the integral-relation theory are listed in table III for all the shapes given in table II.

The disparity between pressure distributions given by different theories for the same shape is illustrated in figure 7. Presented are the pressure distributions calculated from Newtonian theory and from integral-relation theory at a Mach number of 3 for the Newtonian-derived tension-shell shape for $Z = 0.65$ and $r_n = 0.05r_b$. The results are typical for all shapes considered herein and indicate considerable difference in predicted trends. For example, pressures obtained from the integral-relation theory decrease from the stagnation point and are substantially higher over most of the surface with respect to the Newtonian values, whereas the Newtonian pressures increase from the nose-cap tension-shell juncture.

The initial Newtonian-derived tension-shell shape, the final-iterated (integral-relation) shape at $M_\infty = 3.0$ and the pressure distributions used in the derivations are shown in figures 8(a), 8(b), and 8(c) for $Z = 0.50$, 0.65, and 0.80, respectively. The final-iterated shapes which are shown met the convergence criteria after only four iterations. This rapid convergence is demonstrated in figure 8(b) for the $Z = 0.65$ shape. Typically, a substantial decrease in the length of the shape occurred with the first iteration. Second, third, and fourth iterations resulted in consecutively smaller differences in length as shown by the detail in figure 8(b). The pressure distributions converged in a similar manner, but smaller differences were obtained between successive iterations. The integral-relation pressure values produced by the first- and fourth-iterated shapes are similar and are only slightly larger than the integral-relation pressures calculated for the initial Newtonian shape.

A comparison of figures 8(a), 8(b), and 8(c) shows that the changes in pressures obtained from integral-relation theory are small for the changes in shape considered. In contrast, the Newtonian pressures show a strong sensitivity to shape change.

Effects of nose radius and Mach number on shapes and pressure distributions derived from integral-relation theory.- Since the integral-relation pressure distributions and the derived tension-shell shapes are somewhat dependent on the assumed nose radius and the free-stream Mach number, it is desirable to document the effects of these variables. Therefore, pressure distributions and tension-shell shapes were computed for $Z = 0.65$ at a Mach number of 3.0 with $r_n/r_b = 0.05$, 0.20, and 0.56 and for Mach numbers of 2.5, 3.0, 5.0, and 7.0 with $r_n/r_b = 0.05$. The effects resulting from the nose radius and Mach number variations are shown in figures 9 and 10, respectively.

In figure 9, the only visible effect of nose radius on the pressure distribution is a slight perturbation which occurs in the region of the spherical nose cap. Overall effects

are small, thus, variations in nose bluntness have little effect on the flow characteristics of bluff tension-shell shapes. This result is in agreement with conclusions presented in reference 15 for large-angle cones with the sonic point located at the shoulder. Therefore, tension-shell shapes that are computed from the integral-relation pressure distributions are relatively insensitive to the nose radius used in obtaining the pressure distribution.

In contrast to these results, figure 10 shows that Mach number affects both the pressure distribution and the tension-shell shape. An increase in Mach number results in a reduced static-pressure loading and a shorter tension-shell shape, but both the pressure distribution and the tension-shell shape approach a limiting value as the Mach number increases. Since aerodynamic decelerators are used over a finite Mach number range, a tension-shell shape derived for a specific Mach number will be a slightly compromised shape at the other Mach numbers. A comparison of figures 8(b) and 10 shows that the changes in shape that occur within the Mach number range considered herein are not as great as those obtained between Newtonian-derived and integral-relation-derived tension-shell shapes.

Experimental Pressure Distributions

A summary of the experimental pressures obtained from the wind-tunnel tests at $M_\infty = 3.0$ is provided in table IV in pressure coefficient form and is presented graphically in figures 11(a) and 11(b) for the Newtonian- and integral-relation-derived tension-shell shapes for $Z = 0.65$ and $r_n/r_b = 0.20$. The data from both models show excellent repeatability and indicate nearly identical pressure distributions in spite of the difference in the shapes. (See fig. 4.) Thus, the experimental results substantiate the conclusion from the computed integral-relation pressure distributions of figure 8 that the pressure distribution for a bluff tension-shell shape is relatively insensitive to significant changes in the tension-shell shapes. For the shapes of figure 11 and table IV, relatively high and nearly constant pressures are generated along the front surface to a value of $r/r_b \approx 0.75$ before the flow expansion around the sharp corner at the base influences the pressures. Nearly constant values of pressure that are less than the free-stream static pressure are obtained along the rear surface.

Comparison of Theory and Experiment

Pressure distributions.- Figure 11 includes curves of the pressures obtained from integral-relation and Newtonian theories. As the figure shows, the experimental data favor the curves given by the integral-relation theory. The agreement between experiment and integral-relation theory is excellent over the nose cap and is within 9 percent over the remaining portion of the Newtonian-derived shape (fig. 11(a)) and within 7 percent

for the integral-relation-derived shape (fig. 11(b)). The experimentally determined pressures lie above the integral-relation curve downstream of the nose-cap juncture, and the maximum deviation between experiment and theory occurs at a value of $r/r_b \approx 0.90$. Thus, integral-relation theory gives a much better representation of the aerodynamic loading on bluff tension-shell shapes than Newtonian theory and is recommended for use in design applications.

Shapes determined from experimental pressures.- The experimental pressure distributions of figure 11 were used in the linear-membrane computer program to determine shapes for comparison with the theoretically determined shapes. The coordinates of the experimental shapes and their corresponding experimental pressure distribution in terms of the nondimensional membrane pressure differential P are given in table V. The pressures are an average of those obtained from the two tests conducted on each wind-tunnel model. These experimental shapes and their pressure distributions are compared with corresponding Newtonian-derived and integral-relation-derived shapes and pressure distributions in figure 12. In this figure, unlike figure 11, the experimental pressure values are generally less than the pressure values obtained from integral-relation theory because the experimental values of the parameter P were evaluated by using measured values of base pressure, whereas the values of P determined from integral-relation theory were evaluated by assuming zero base pressure. The agreement between the experimental and integral-relation values of P, however, is within 4 percent. The tension-shell shapes derived from the experimental pressures differ by less than 2 percent and should be representative of shapes obtained under true aerodynamic loading. Moreover, these shapes are in excellent agreement with the integral-relation-derived shape. Consequently, a more accurate representation of a bluff tension-shell shape can be obtained from pressures determined from integral-relation theory rather than from Newtonian theory.

Drag coefficients.- One of the criteria which govern the final selection of a decelerator shape is the drag coefficient. In table VI, the drag coefficients predicted by Newtonian and integral-relation theories for tension-shell shapes for $Z = 0.65$ and $r_n/r_b = 0.20$ are compared with drag coefficients obtained by integrating the experimental pressure distributions of figure 10. All drag coefficients are based on a free-stream static base pressure to provide a common basis for comparison. The drag coefficients predicted by Newtonian theory are up to 13 percent greater than experimental values, whereas the drag coefficients predicted by integral-relation theory are 6 percent less than experimental values. Thus, conservative and more accurate estimates are obtained from integral-relation theory.

CONCLUSIONS

A study of the application of Newtonian and integral-relation theories to the determination of the shapes and pressure distributions of bluff tension shells and a comparison of these results with experimental results has shown the following:

1. Tension-shell shapes that are derived by using pressure distributions predicted by integral-relation theory are substantially shorter than shapes derived by using Newtonian theory.

2. Although the pressure distributions predicted by integral-relation theory are somewhat dependent on model nose radius and Mach number, the differences in the integral-relation-derived tension-shell shapes attributable to various nose radii and Mach numbers are considerably less than those noted between Newtonian- and integral-relation-derived tension-shell shapes.

3. Experimental pressure distributions were in good agreement with theoretical pressure distributions predicted by integral-relation theory but showed poor agreement with pressure distributions predicted by Newtonian theory.

4. Tension-shell shapes derived by using the experimental pressure distributions were in good agreement with the corresponding integral-relation-derived tension-shell shape but were in poor agreement with the Newtonian-derived tension-shell shape.

5. Drag coefficients predicted by integral-relation theory were approximately 6 percent less than experimental values, whereas Newtonian drag coefficients were up to 13 percent greater than experimental values.

Langley Research Center,
National Aeronautics and Space Administration,
Langley Station, Hampton, Va., September 9, 1969.

APPENDIX

COMPUTER PROGRAM FOR DETERMINATION OF TENSION-SHELL SHAPES

This appendix contains the Fortran IV source program listing for the derivation of tension-shell structures of revolution subject to linear-membrane theory and axisymmetric pressure distribution. The following definitions are used in the program and are defined below or in the list of symbols:

Fortran IV Name	Definition
Z	Z
ALPHA	α
THETAD	limiting configuration slope, deg
THE(J)	radial position array, R
P(J)	pressure distribution array, P
J	indexing parameter
K	indexing parameter
DR	ΔR
THET	θ, deg
RO	R
YO	x/r_b

The following printout is the program listing.

APPENDIX

```
C       PROGRAM FOR CALCULATION OF TENSION SHELL SHAPES
  100 FORMAT(1X2HZ=E16.8,2X6HALPHA=E16.8,2X7HTHETAD=E16.8)
  101 FORMAT(8X5HTHETA8X2HRO8X2HYO12X2HPO)
    1 FORMAT(3E16.8)
    2 FORMAT(2E16.8)
   20 FORMAT(4E16.8)
      DIMENSION THE(500),P(500)
   13 READ(5,1)Z,ALPHA,THETAD
      READ(5,2)(THE(J),P(J),J=1,500)
      DEG=57.295780
      THETAS=1.5707962
      THETAR=THETAD/DEG
      RAN=1.5707000
      J=1
      RO=THE(J)
      DRO=.005
      DR=DRO
   25 THETA=THETAS
      DTHET=THETA
      R=RO
      YO=0.
      K=1
      WRITE(6,100)Z,ALPHA,THETAD
      WRITE(6,101)
      THET=THETA*DEG
      WRITE(6,20)THET,RO,YO,PO
      PUNCH 2,THETA,RO
      L=1
C       COMPARISON OF ANGLES
    3 IF(R.LT.THE(J).AND.R.GT.THE(J+1))GO TO 4
      IF(R.EQ.THE(J))GO TO 5
      IF(R.EQ.THE(J+1))GO TO 6
      IF(R.LT.THE(J+1))GO TO 7
      IF(R.GT.THE(J))GO TO 8
C       INTERPOLATION FOR THETA AND PRESSURE
    4 DOG=(R-THE(J))/(THE(J+1)-THE(J))
      PO=P(J)+(P(J+1)-P(J))*DOG
      GO TO 9
    5 PO=P(J)
      GO TO 9
    6 PO=P(J+1)

      GO TO 9
    7 J=J+1
      GO TO 3
    8 J=J-1
      GO TO 3
C       RUNG-KUTTA INTEGRATION
    9 IF(R.LE.0)GO TO 23
      ER=R**(1.-ALPHA)
      IF(THETA.GT.RAN)A=0.
      IF(THETA.GT.RAN)C=2.*Z*ER*PO
      IF(THETA.GT.RAN)GO TO 14
      TAN=SIN(THETA)/COS(THETA)
      A=-DR*ALPHA/(R*TAN)
      C=2.*Z*ER*PO/SIN(THETA)
```

```
   14 IF(K.EQ.2)GO TO 10
      IF(K.EQ.3)GO TO 11
      IF(K.EQ.4)GO TO 12
      A1=A-DR*C
      IF(THETA.GT.RAN)B1=0.
      IF(THETA.GT.RAN)GO TO 15
      B1=DR/TAN
   15 R=RO-DR/2.
      THETA=DTHET+A1/2.
      K=K+1
      GO TO 3
   10 A2=A-DR*C
      IF(THETA.GT.RAN)B2=0.
      IF(THETA.GT.RAN)GO TO 16
      B2=DR/TAN
   16 K=K+1
      THETA=DTHET+A2/2.
      GO TO 3
   11 A3=A-DR*C
      IF(THETA.GT.RAN)B3=0.
      IF(THETA.GT.RAN)GO TO 17
      B3=DR/TAN
   17 K=K+1
      R=RO-DR
      THETA=DTHET+A3
      IF(R.LE.0)C=0
      IF(R.LE.0)GO TO 12
      GO TO 3
   12 A4=A-DR*C

      IF(THETA.GT.RAN)B4=0.
      IF(THETA.GT.RAN)GO TO 18
      B4=DR/TAN
   18 DELTA=1./6.*(A1+2.*A2+2.*A3+A4)
      DTHET=DTHET+DELTA
      THETA=DTHET
      THET=THETA*DEG
      RO=RO-DR
      DY=1./6.*(B1+2.*B2+2.*B3+B4)
      YO=YO+DY
C     PRINT RESULTS
      WRITE(6,20)THET,RO,YO,PO
      PUNCH 2,THETA,RO
      K=1
      IF(R.LE.0)GO TO 23
      IF(THETA.GT.THETAR)GO TO 3
   23 CONTINUE
      STOP
      END
```

REFERENCES

1. Anderson, Melvin S.; Robinson, James C.; Bush, Harold G.; and Fralich, Robert W.: A Tension Shell Structure for Application to Entry Vehicles. NASA TN D-2675, 1965.

2. Deveikis, William D.; and Sawyer, James Wayne: Aerodynamic Characteristics of Tension Shell Shapes at Mach 3.0. NASA TN D-3633, 1966.

3. Robinson, James C.; and Jordan, Alfred W.: Exploratory Experimental Aerodynamic Investigation of Tension Shell Shapes at Mach 7.0. NASA TN D-2994, 1965.

4. Bernot, Peter T.: Longitudinal Stability Characteristics of Several Proposed Planetary Entry Vehicles at Mach 6.73. NASA TN D-2785, 1965.

5. Creel, Theodore R.: Longitudinal Aerodynamic Characteristics of a Tension Shell Entry Configuration at Mach 20.0. NASA TN D-3541, 1966.

6. Anderson, Roger A.: Structures Technology – 1964. Astronaut. Aeronaut., vol. 2, no. 12, Dec. 1964, pp. 14-20.

7. Roberts, Leonard: Entry Into Planetary Atmospheres. Astronaut. Aeronaut., vol. 2, no. 10, Oct. 1964, pp. 22-29.

8. Sawyer, James Wayne; and Deveikis, William D.: Effects of Configuration Modifications on Aerodynamic Characteristics of Tension Shell Shapes at Mach 3.0. NASA TN D-4080, 1967.

9. Harris, Charles D.: Transonic Aerodynamic Investigation of Tension Shell and Blunted 100° Conical Shapes for Unmanned Entry Vehicles. NASA TN D-3700, 1966.

10. Sawyer, James Wayne: Comparison of the Mach 3.0 Aerodynamic Characteristics of Tension String, Tension Shell, and 120° Conical Shapes. NASA TN D-4360, 1968.

11. Jones, Robert A.; Bushnell, Dennis M.; and Hunt, James L: Experimental Flow Field and Heat-Transfer Investigation of Several Tension Shell Configurations at a Mach Number of 8. NASA TN D-3800, 1967.

12. South, Jerry C., Jr.: Calculation of Axisymmetric Supersonic Flow Past Blunt Bodies with Sonic Corners, Including a Program Description and Listing. NASA TN D-4563, 1968.

13. Comm. on Metric Pract.: ASTM Metric Practice Guide. NBS Handbook 102, U.S. Dep. Com., Mar. 10, 1967.

14. Schaefer, William T., Jr.: Characteristics of Major Active Wind Tunnels at the Langley Research Center NASA TM X-1130, 1965.

15. Ward, L. Christopher; and Pugh, Philip G.: Shock Standoff Distances of Blunt and Sharp Cones. AIAA J. vol. 6, no. 10, Oct. 1968, pp. 2018-2019.

TABLE I.- COORDINATES AND ORIFICE LOCATIONS FOR NEWTONIAN- AND INTEGRAL-RELATION-DERIVED PRESSURE DISTRIBUTION MODELS

Orifice	x/r_b for –	r/r_b for –	x/r_b for –	r/r_b for –	Orifice	x/r_b for –	r/r_b for –	x/r_b for –	r/r_b for –
	Newtonian shape		Integral-relation shape			Newtonian shape		Integral-relation shape	
1	0.4113	0	0.3588	0	26	0.0811	0.625	0.0630	0.625
2	.4097	.025	.3572	.025	27	.0712	.650	.0549	.650
3	.4049	.050	.3525	.050	28	.0619	.675	.0474	.675
4	.3967	.075	.3442	.075	29	.0532	.700	.0404	.700
5	.3845	.100	.3320	.100	30	.0450	.725	.0339	.725
6	.3680	.125	.3167	.125	31	.0375	.750	.0279	.750
7	.3510	.150	.3010	.150	32	.0306	.775	.0226	.775
8	.3341	.175	.2854	.175	33	.0244	.800	.0178	.800
9	.3174	.200	.2701	.200	34	.0188	.825	.0135	.825
10	.3008	.225	.2550	.225	35	.0139	.850	.0099	.850
11	.2845	.250	.2401	.250	36	.0098	.875	.0068	.875
12	.2685	.275	.2256	.275	37	.0063	.900	.0043	.900
13	.2527	.300	.2114	.300	38	.0036	.925	.0024	.925
14	.2371	.325	.1975	.325	39	.0016	.950	.0010	.950
15	.2219	.350	.1839	.350	40	.0004	.975	.0002	.975
16	.2071	.375	.1707	.375	41	.0001	.987	.0001	.987
17	.1925	.400	.1579	.400		0	1.000	0	1.000
18	.1784	.425	.1456	.425	42	(*)	.987	(*)	.987
19	.1646	.450	.1336	.450	43	(*)	.900	(*)	.900
20	.1513	.475	.1221	.475	44	(*)	.800	(*)	.800
21	.1384	.500	.1111	.500	45	(*)	.700	(*)	.700
22	.1259	.525	.1005	.525	46	(*)	.600	(*)	.600
23	.1140	.550	.0904	.550	47	(*)	.500	(*)	.500
24	.1025	.575	.0808	.575	48	(*)	.400	(*)	.400
25	.0915	.600	.0716	.600	49	(*)	.300	(*)	.300

*Orifices installed on base of model.

TABLE II.- COORDINATES FOR NEWTONIAN- AND INTEGRAL-RELATION-DERIVED TENSION-SHELL SHAPES

(a) Newtonian shapes $M_\infty = \infty$; $\gamma = 1.00$; $r_n/r_b = 0$

(b) Integral-relation shapes ($\gamma = 1.40$)

r/r_b	x/r_b for –		
	Z = 0.50	Z = 0.65	Z = 0.80
0	0.3430	0.4546	0.5734
.050	.3169	.4198	.5290
.100	.2910	.3852	.4849
.150	.2654	.3510	.4414
.200	.2402	.3174	.3986
.250	.2156	.2845	.3569
.300	.1917	.2527	.3164
.350	.1686	.2219	.2775
.400	.1464	.1925	.2404
.450	.1254	.1646	.2052
.500	.1055	.1384	.1722
.550	.0870	.1140	.1416
.600	.0700	.0915	.1136
.650	.0545	.0712	.0882
.700	.0407	.0532	.0658
.750	.0288	.0375	.0463
.800	.0187	.0244	.0301
.850	.0107	.0139	.0172
.900	.0048	.0063	.0077
.950	.0012	.0016	.0020
1.000	0	0	0

x/r_b for –							
Z = 0.50 M_∞ = 3.00 r_n/r_b = 0.05	Z = 0.65 M_∞ = 2.50 r_n/r_b = 0.05	Z = 0.65 M_∞ = 3.00 r_n/r_b = 0.05	Z = 0.65 M_∞ = 5.00 r_n/r_b = 0.05	Z = 0.65 M_∞ = 7.00 r_n/r_b = 0.05	Z = 0.65 M_∞ = 3.00 r_n/r_b = 0.20	Z = 0.65 M_∞ = 3.00 r_n/r_b = 0.56	Z = 0.80 M_∞ = 3.00 r_n/r_b = 0.05
0.2928	0.4081	0.3971	0.3865	0.3843	0.3972	0.3973	0.5211
.2695	.3748	.3647	.3550	.3531	.3648	.3648	.4769
.2463	.3417	.3326	.3238	.3221	.3326	.3327	.4332
.2235	.3092	.3010	.2931	.2916	.3010	.3010	.3903
.2012	.2774	.2701	.2631	.2618	.2701	.2701	.3486
.1794	.2466	.2401	.2340	.2329	.2401	.2402	.3085
.1584	.2170	.2113	.2061	.2050	.2114	.2114	.2702
.1383	.1888	.1839	.1794	.1785	.1839	.1839	.2340
.1192	.1622	.1579	.1541	.1534	.1579	.1580	.2000
.1011	.1372	.1336	.1304	.1298	.1336	.1337	.1684
.0843	.1141	.1111	.1084	.1079	.1111	.1111	.1394
.0688	.0929	.0904	.0882	.0878	.0904	.0904	.1129
.0547	.0736	.0716	.0699	.0696	.0716	.0717	.0892
.0420	.0565	.0549	.0536	.0534	.0549	.0550	.0682
.0309	.0415	.0404	.0394	.0392	.0404	.0404	.0499
.0215	.0288	.0279	.0272	.0271	.0279	.0280	.0345
.0137	.0183	.0178	.0173	.0172	.0178	.0178	.0219
.0076	.0102	.0099	.0096	.0096	.0099	.0099	.0121
.0033	.0045	.0043	.0042	.0041	.0043	.0043	.0053
.0008	.0011	.0010	.0010	.0009	.0010	.0010	.0013
0	0	0	0	0	0	0	0

TABLE III.- INTEGRAL-RELATION PRESSURE DISTRIBUTIONS AND DRAG COEFFICIENTS FOR TENSION-SHELL SHAPES

(a) Newtonian shapes ($M_\infty = \infty$; $\gamma = 1.00$; $r_n/r_b = 0$)

(b) Integral-relation shapes ($\gamma = 1.40$)

r/r_b	p for –		
	Z = 0.50	Z = 0.65	Z = 0.80
0	1.9142	1.9142	1.9142
.050	1.8899	1.8729	1.8309
.100	1.8782	1.8531	1.7943
.150	1.8659	1.8354	1.7798
.200	1.8536	1.8203	1.7663
.250	1.8405	1.8072	1.7564
.300	1.8301	1.7956	1.7487
.350	1.8188	1.7851	1.7423
.400	1.8075	1.7752	1.7365
.450	1.7961	1.7656	1.7308
.500	1.7843	1.7557	1.7248
.550	1.7717	1.7452	1.7178
.600	1.7578	1.7335	1.7093
.650	1.7419	1.7198	1.6987
.700	1.7231	1.7032	1.6849
.750	1.7000	1.6823	1.6666
.800	1.6700	1.6548	1.6415
.850	1.6289	1.6163	1.6056
.900	1.5674	1.5578	1.5500
.950	1.4592	1.4538	1.4496
1.000	1.0114	1.0114	1.0114
C_D...	1.519	1.500	1.478

p for –							
Z = 0.50 M_∞ = 3.00 r_n/r_b = 0.05	Z = 0.65 M_∞ = 2.50 r_n/r_b = 0.05	Z = 0.65 M_∞ = 3.00 r_n/r_b = 0.05	Z = 0.65 M_∞ = 5.00 r_n/r_b = 0.05	Z = 0.65 M_∞ = 7.00 r_n/r_b = 0.05	Z = 0.65 M_∞ = 3.00 r_n/r_b = 0.20	Z = 0.65 M_∞ = 3.00 r_n/r_b = 0.56	Z = 0.80 M_∞ = 3.00 r_n/r_b = 0.05
1.9142	1.9485	1.9142	1.8657	1.8526	1.9143	1.9143	1.9142
1.8944	1.9110	1.8802	1.8348	1.8218	1.9013	1.9095	1.8480
1.8848	1.8963	1.8651	1.8184	1.8048	1.8639	1.8984	1.8211
1.8745	1.8816	1.8504	1.8039	1.7905	1.8487	1.8798	1.8034
1.8640	1.8682	1.8373	1.7917	1.7788	1.8368	1.8552	1.7909
1.8534	1.8560	1.8255	1.7813	1.7690	1.8254	1.8260	1.7817
1.8429	1.8449	1.9148	1.7721	1.7605	1.8148	1.8077	1.7743
1.8324	1.8344	1.8048	1.7638	1.7528	1.8049	1.8019	1.7681
1.8218	1.8243	1.7953	1.7558	1.7455	1.7953	1.7940	1.7622
1.8108	1.8143	1.7857	1.7478	1.7374	1.7857	1.7852	1.7562
1.7993	1.8040	1.7757	1.7394	1.7303	1.7758	1.7756	1.7496
1.7868	1.7930	1.7650	1.7295	1.7215	1.7650	1.7650	1.7418
1.7728	1.7808	1.7528	1.7191	1.7111	1.7529	1.7516	1.7325
1.7568	1.7668	1.7386	1.7060	1.6986	1.7387	1.7388	1.7208
1.7378	1.7501	1.7214	1.6897	1.6827	1.7215	1.7216	1.7076
1.7141	1.7294	1.6997	1.6685	1.6620	1.6998	1.7000	1.6864
1.6836	1.7025	1.6711	1.6399	1.6338	1.6713	1.6715	1.6599
1.6415	1.6657	1.6313	1.5993	1.5935	1.6315	1.6317	1.6222
1.5785	1.6106	1.5709	1.5367	1.5308	1.5712	1.5714	1.5642
1.4674	1.5127	1.4633	1.4248	1.4185	1.4638	1.4787	1.4597
1.0114	1.0295	1.0114	0.9857	0.9788	1.0114	1.0114	1.0114
1.532	1.480	1.516	1.582	1.602	1.516	1.517	1.498

TABLE IV.- EXPERIMENTAL PRESSURE DATA FOR TENSION-SHELL SHAPES

FOR $Z = 0.65$ AND $r_n/r_b = 0.20$

Orifice	C_p for –				Orifice	C_p for –			
	Newtonian shape		Integral-relation shape			Newtonian shape		Integral-relation shape	
	Test 1	Test 2	Test 1	Test 2		Test 1	Test 2	Test 1	Test 2
1	1.756	1.757	1.758	1.755	26	1.645			1.650
2	1.752			1.751	27	1.649	1.652	1.658	1.655
3	1.739	1.741	1.747	1.746	28	1.638	1.637	1.640	1.643
4	1.720	1.720	1.722	1.723	29	1.641	1.640	1.645	1.645
5	1.702	1.704	1.718	1.718	30	1.622	1.629	1.630	1.627
6	1.695	1.698	1.707	1.704	31		1.630	1.633	
7	1.694	1.695	1.708	1.708	32	1.617	1.617	1.616	1.618
8	1.686	1.687	1.698	1.697	33	1.613	1.613	1.611	1.610
9	1.694	1.687	1.700	1.699	34	1.592	1.593	1.591	1.588
10	1.679	1.680	1.691	1.690	35	1.581	1.587	1.581	1.575
11	1.679	1.679	1.693	1.692	36	1.559	1.553	1.549	1.554
12	1.674	1.674	1.685	1.685	37	1.539	1.537	1.528	1.528
13	1.674	1.674	1.689	1.690	38	1.492	1.493	1.484	1.484
14	1.670	1.671	1.680	1.679	39	1.446	1.451	1.432	1.426
15	1.671	1.670	1.686	1.686	40	1.325	1.323	1.311	1.314
16	1.667	1.664	1.676	1.679	41	1.202	1.204	1.194	1.192
17	1.666	1.671	1.683	1.682	42	-.067	-.062	-.060	-.072
18	1.660	1.660	1.673	1.672	43	-.078	-.076	-.076	-.078
19	1.662	1.662	1.679	1.678	44	-.077	-.079	-.078	-.078
20	1.657	1.658	1.667	1.668	45	-.095	-.081	-.080	-.096
21	1.664	1.662	1.675	1.677	46	-.093	-.073	-.097	-.087
22	1.654	1.653	1.662	1.663	47	-.057	-.090	-.094	-.072
23	1.657	1.662	1.673	1.667	48	-.076	-.062	-.072	-.089
24		1.649	1.656		49	-.097	-.063	-.098	-.089
25	1.655	1.652	1.661	1.664					

TABLE V.- EXPERIMENTAL PRESSURE DISTRIBUTIONS AND THE DERIVED TENSION-SHELL SHAPES FOR $Z = 0.65$ AND $r_n/r_b = 0.20$

P (a)	r/r_b	x/r_b	P (b)	r/r_b	x/r_b
Experimental configuration I			Experimental configuration II		
1.830	0	0.3958	1.838	0	0.4015
1.815	.050	.3638	1.824	.050	.3680
1.779	.100	.3320	1.798	.100	.3348
1.766	.150	.3007	1.786	.150	.3030
1.758	.200	.2702	1.778	.200	.2721
1.751	.250	.2405	1.772	.250	.2421
1.745	.300	.2119	1.768	.300	.2132
1.742	.350	.1846	1.763	.350	.1857
1.739	.400	.1588	1.760	.400	.1597
1.736	.450	.1345	1.756	.450	.1352
1.734	.500	.1120	1.752	.500	.1125
1.729	.550	.0912	1.747	.550	.0916
1.724	.600	.0724	1.741	.600	.0727
1.717	.650	.0556	1.734	.650	.0558
1.708	.700	.0409	1.723	.700	.0410
1.696	.750	.0283	1.710	.750	.0284
1.680	.800	.0180	1.689	.800	.0180
1.653	.850	.0100	1.658	.850	.0110
1.610	.900	.0043	1.610	.900	.0043
1.510	.950	.0010	1.514	.950	.0010
0.925	1.000	0	.933	1.000	0

[a]Pressure distribution measured on Newtonian tension-shell shape.

[b]Pressure distribution measured on integral-relation tension-shell shape.

TABLE VI.- THEORETICAL AND EXPERIMENTAL DRAG COEFFICIENTS FOR THE NEWTONIAN- AND INTEGRAL-RELATION-DERIVED TENSION-SHELL SHAPES FOR $Z = 0.65$ AND $r_n/r_b = 0.20$

Calculation method	Drag coefficient for –	
	Newtonian shape	Integral-relation shape
Newtonian theory	1.759	1.814
Integral-relation theory	1.500	1.516
Experimental	1.590	1.590

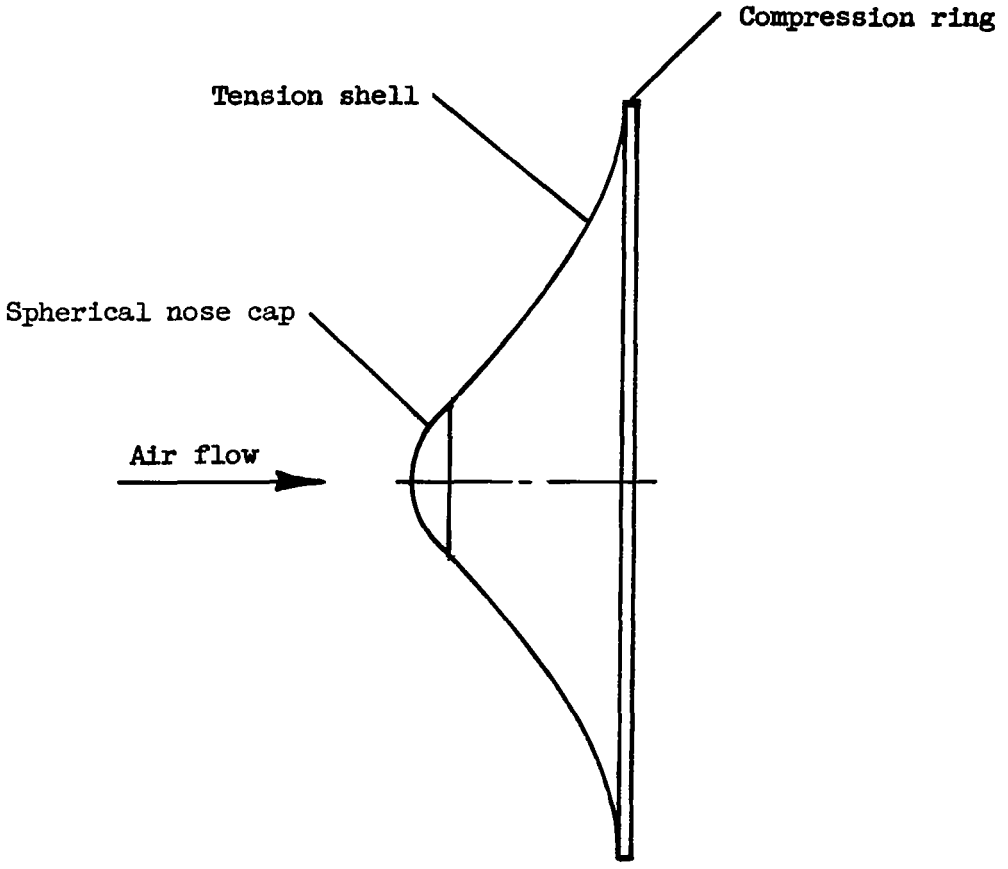

Figure 1.- Typical tension-shell decelerator.

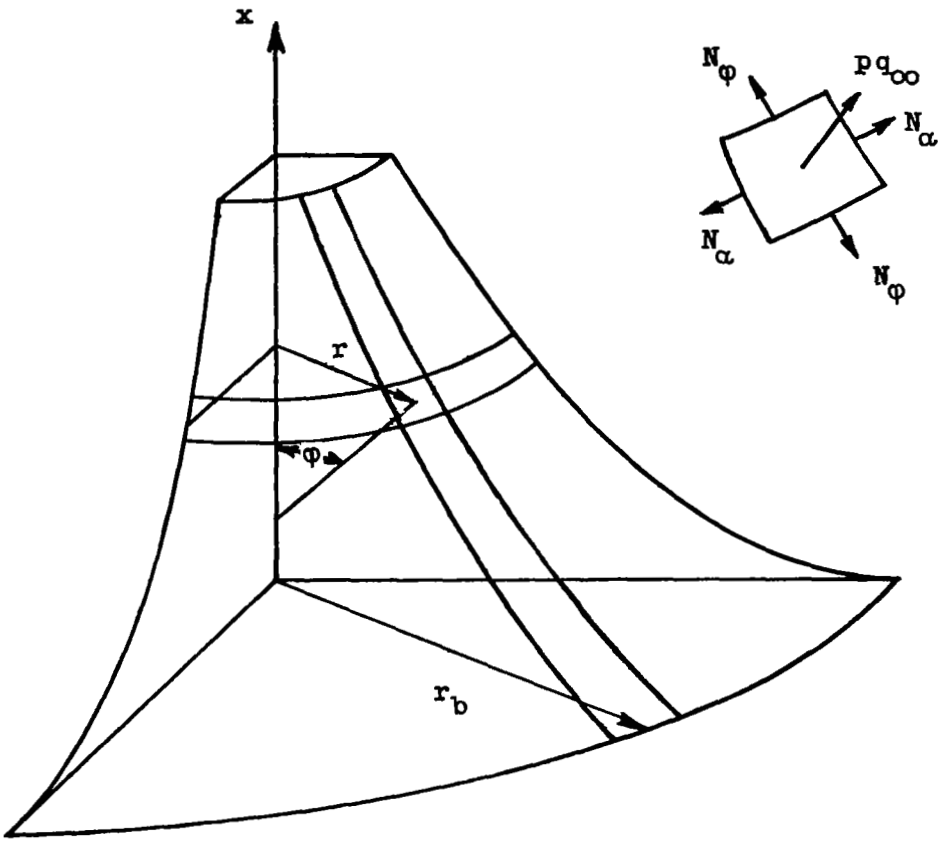

Figure 2.- Tension-shell shape and coordinate system.

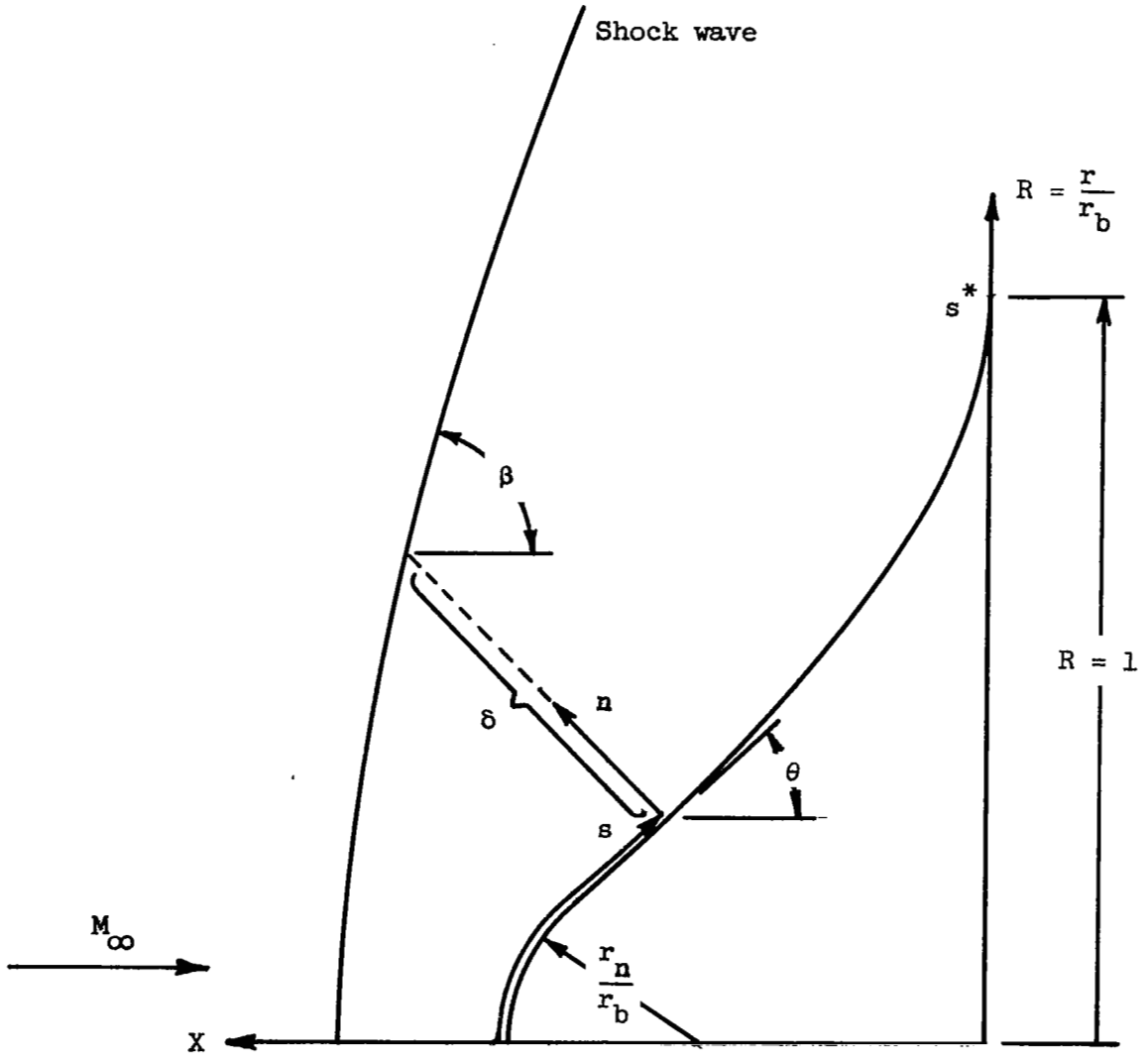

Figure 3.- Geometry and coordinate system for aerodynamic consideration.

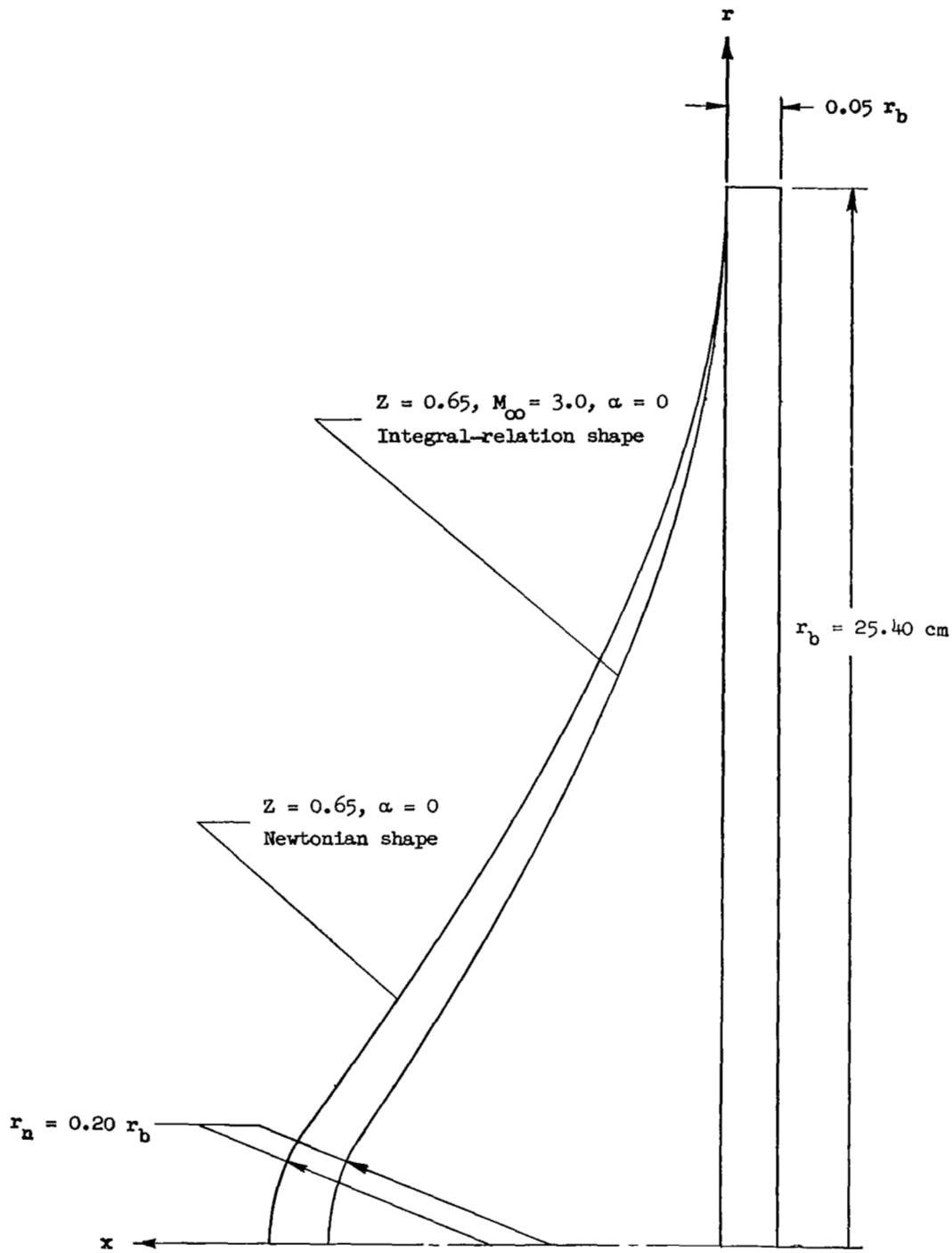

Figure 4.- Details of test models.

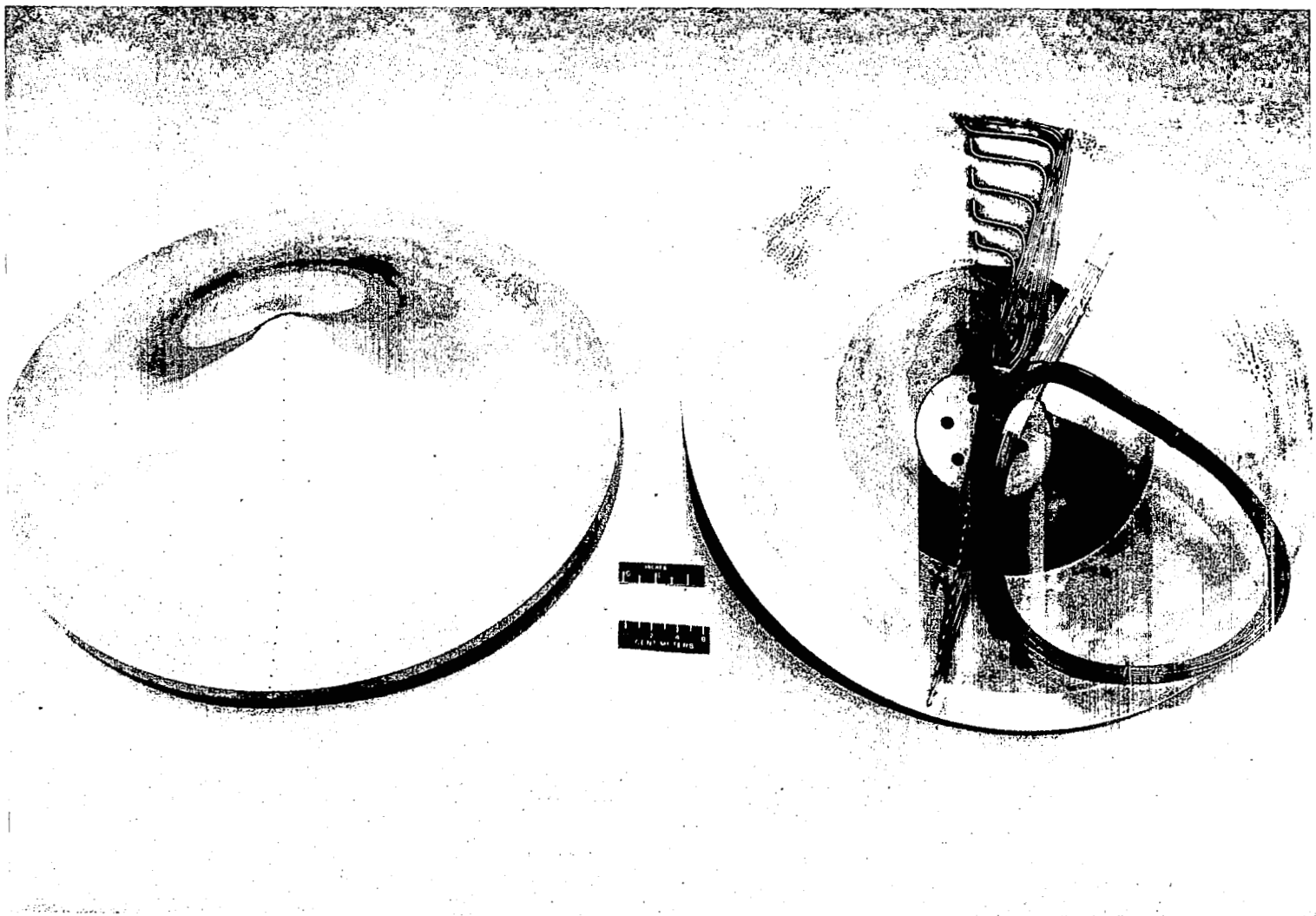

Figure 5.- Photograph of test models.

L-68-7296

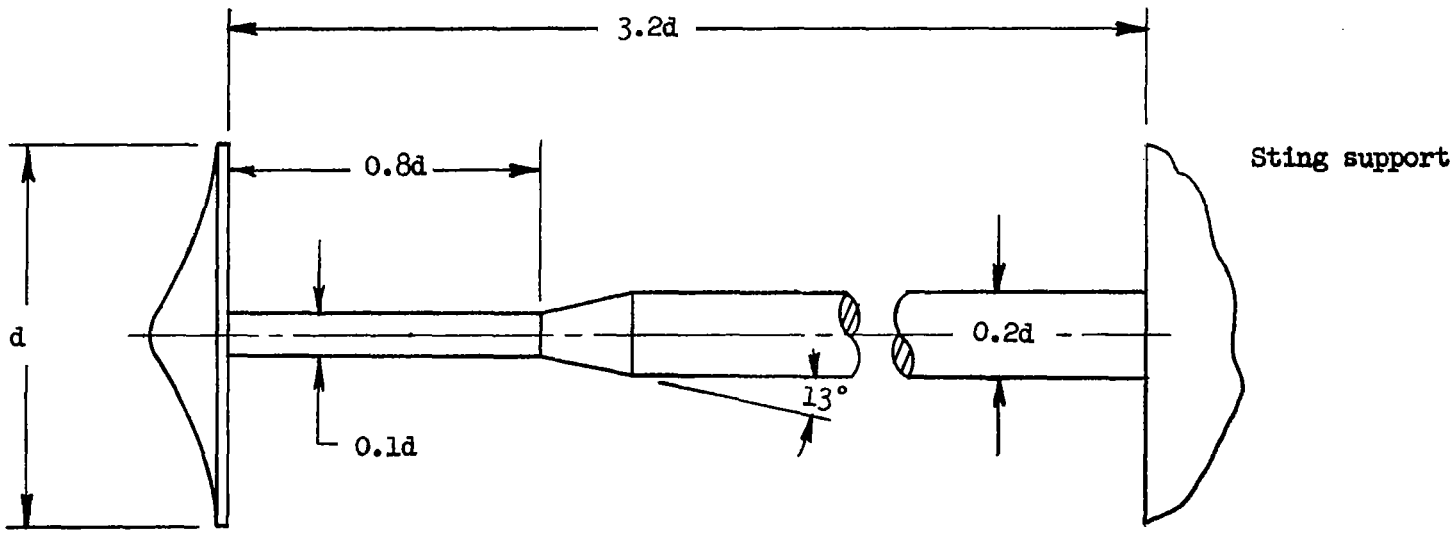

Figure 6.- Illustration of model sting-mount system. d = 50.8 cm.

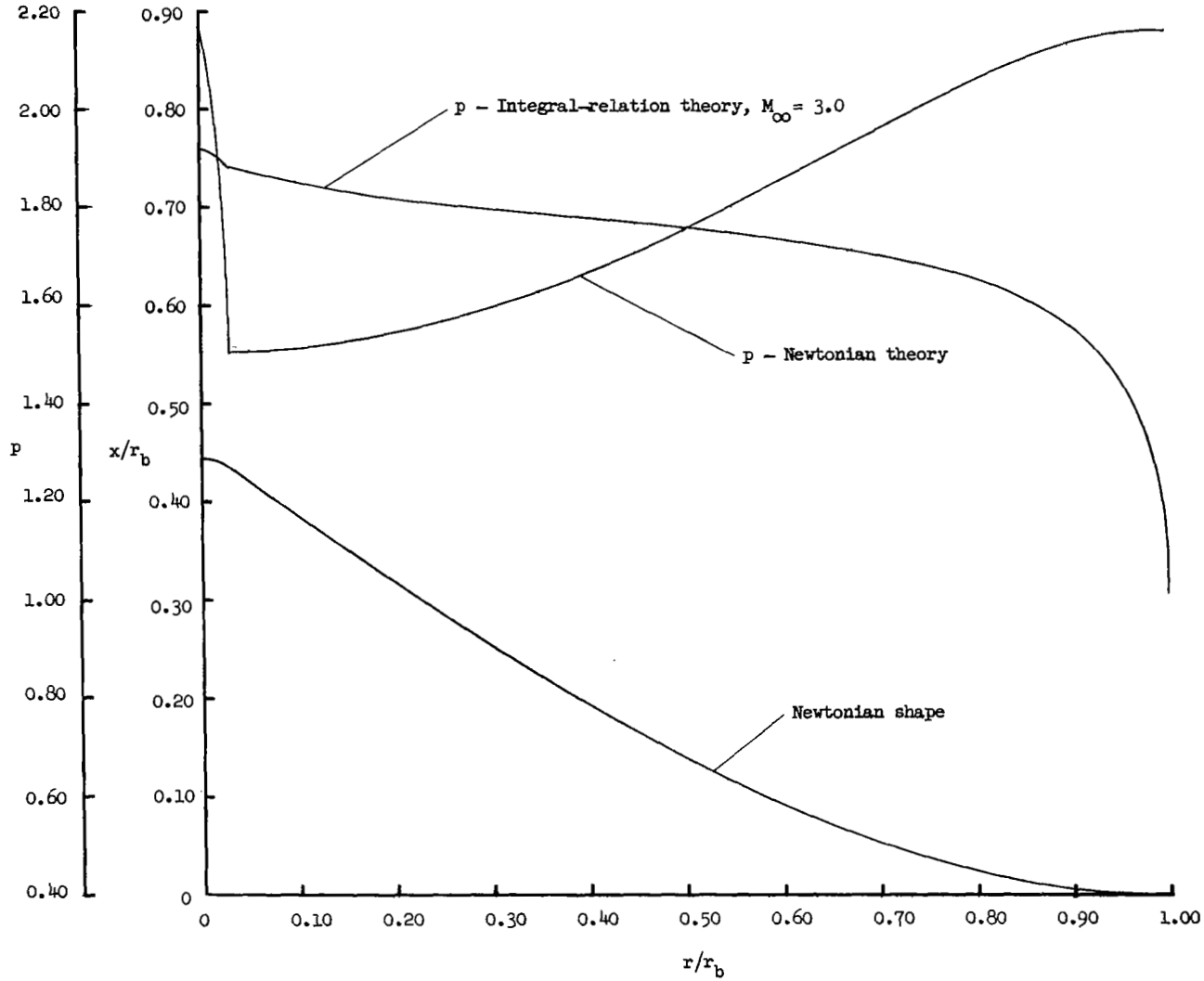

Figure 7.- Theoretical pressure distributions for the Newtonian-derived tension-shell shape for $Z = 0.65$, $r_n/r_b = 0.05$, and $\alpha = 0$.

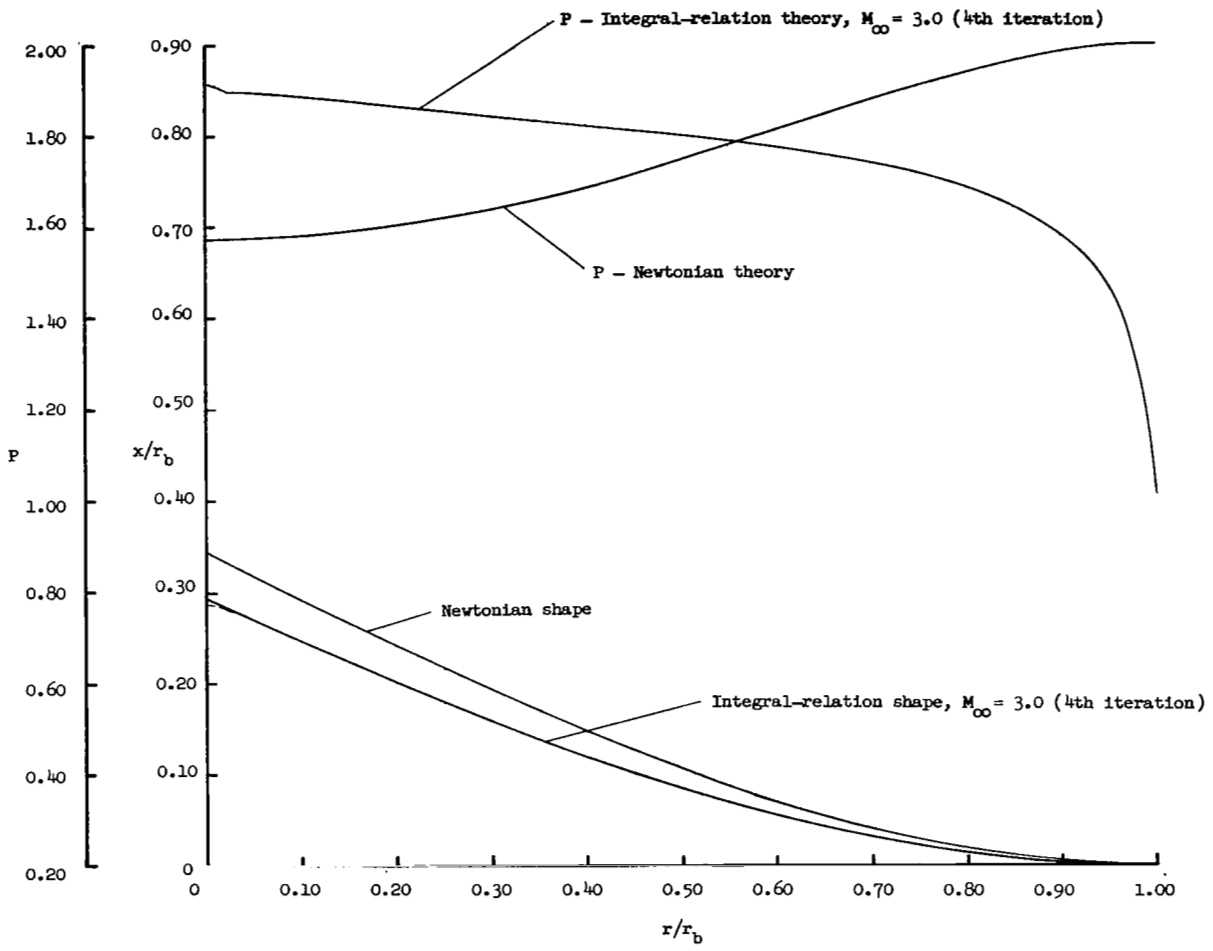

(a) Z = 0.50.

Figure 8.- Comparison of Newtonian and integral-relation pressure distributions and corresponding tension-shell shapes. $\alpha = 0$.

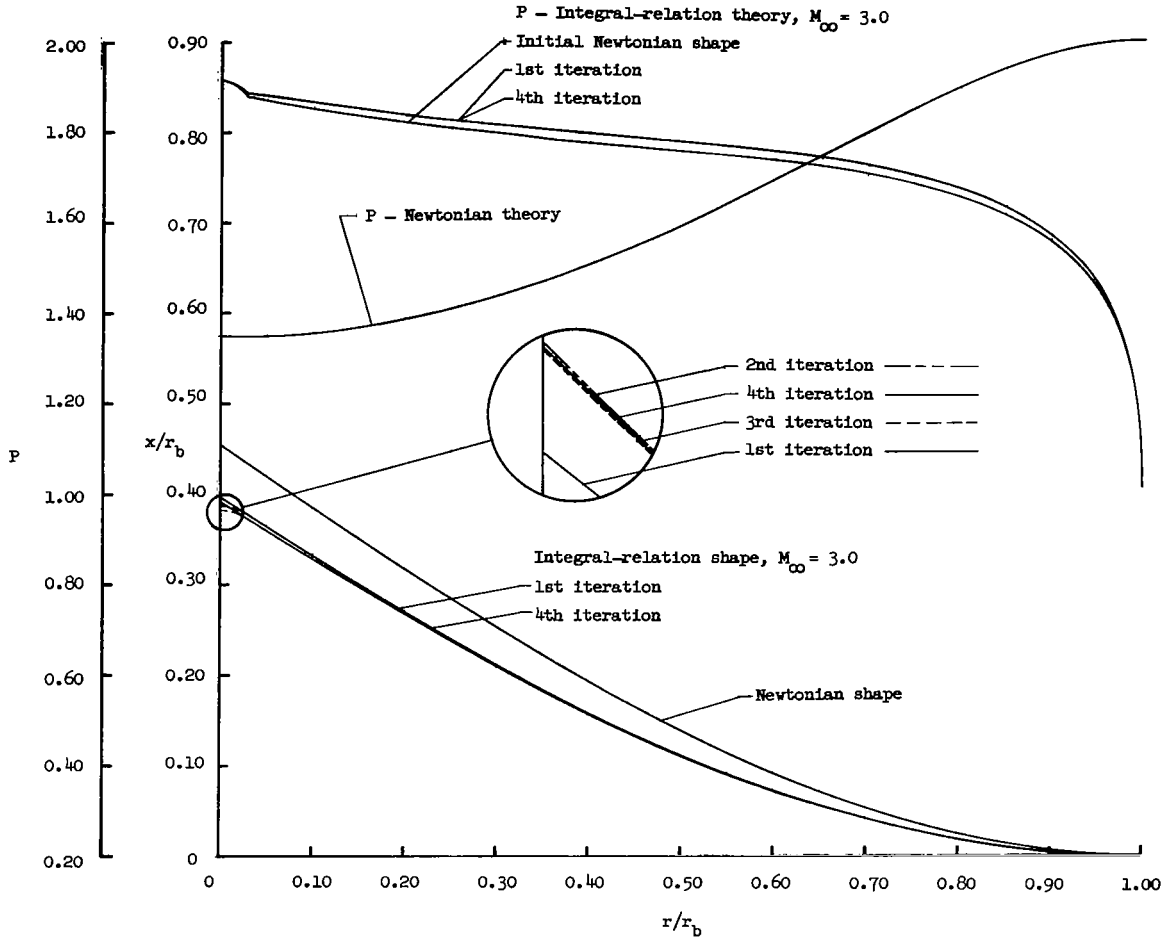

(b) Z = 0.65.

Figure 8.- Continued.

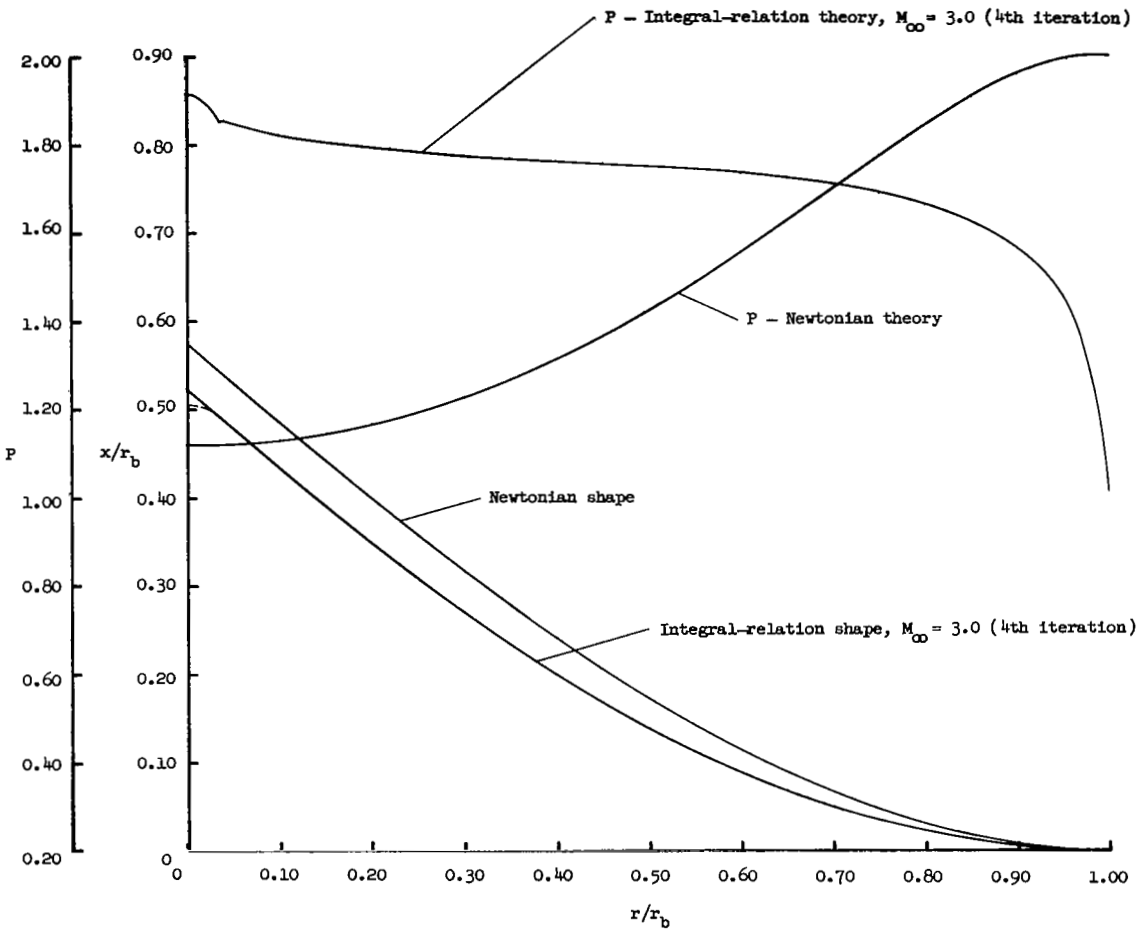

(c) Z = 0.80.

Figure 8.- Concluded.

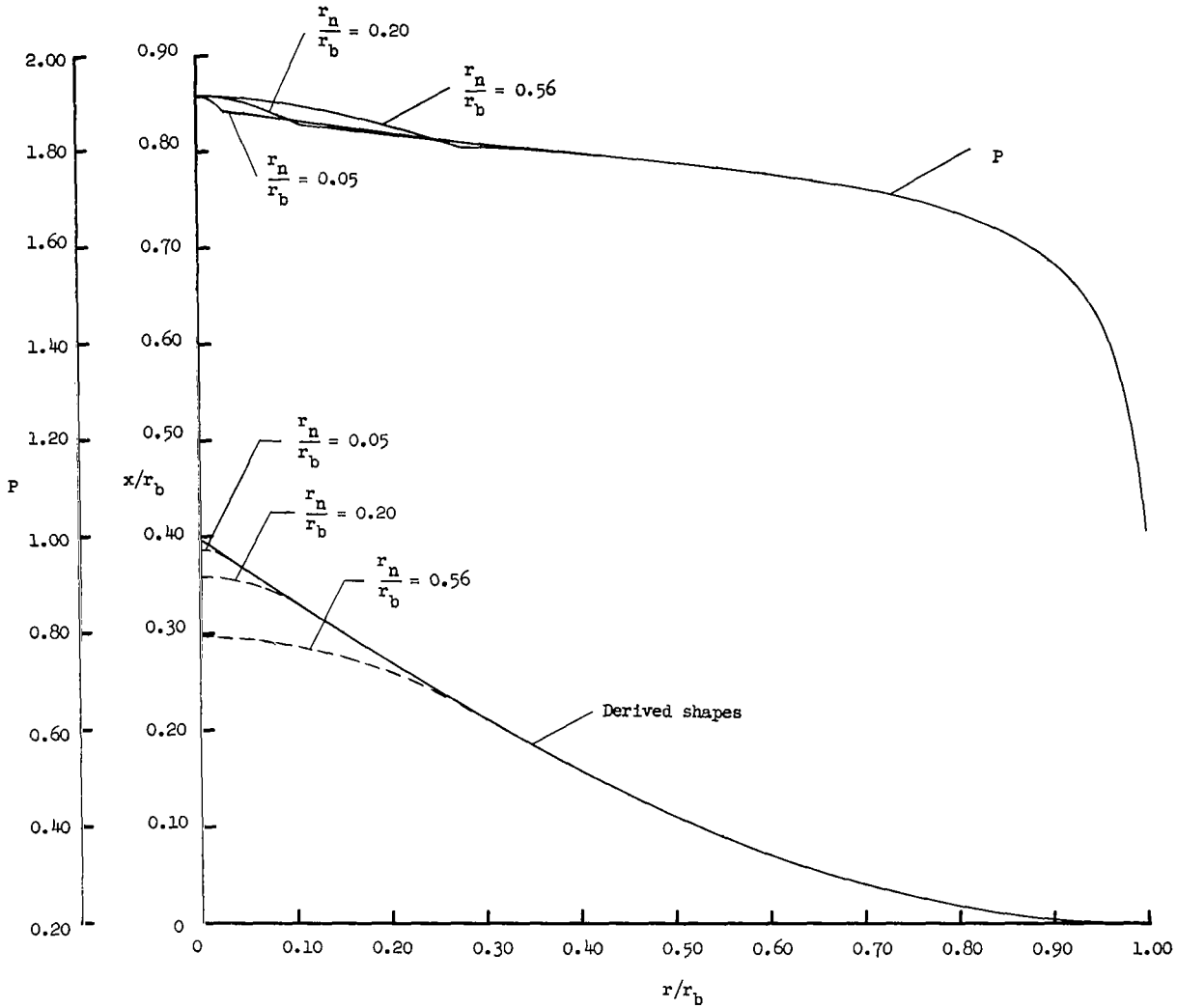

Figure 9.- Effects of nose radius on the integral-relation pressure distributions and derived tension-shell shapes for $Z = 0.65$, $M_\infty = 3.0$, and $\alpha = 0$.

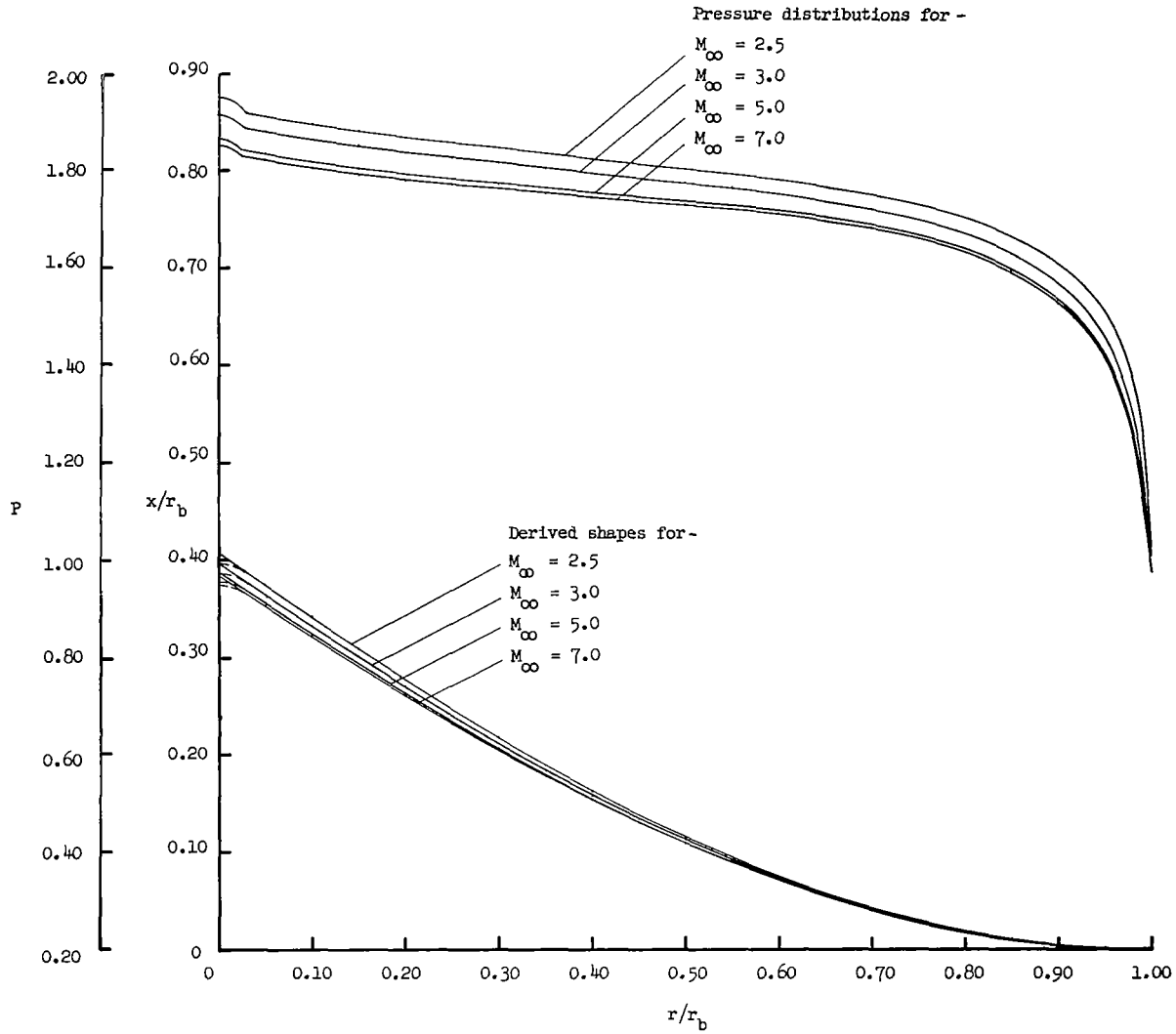

Figure 10.- Effects of Mach number on the integral-relation pressure distributions and derived tension-shell shapes for $Z = 0.65$, $r_n/r_b = 0.05$, and $\alpha = 0$.

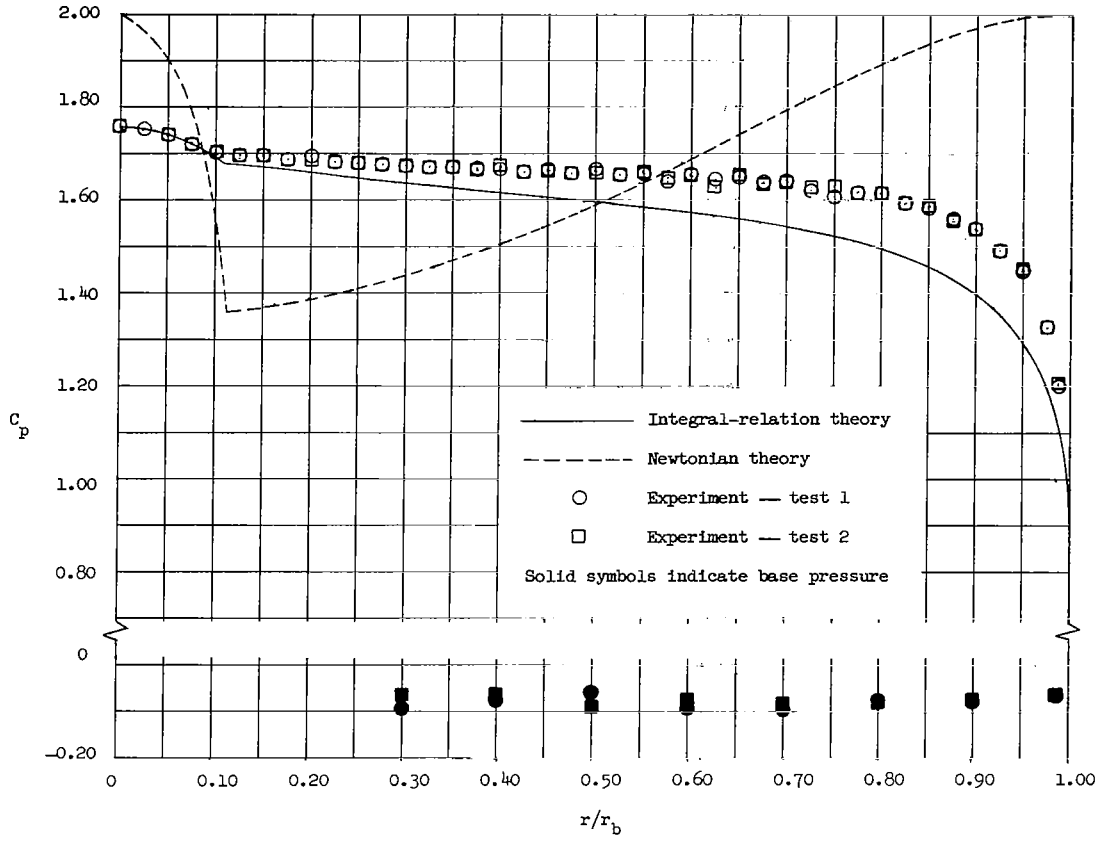

(a) Newtonian-derived shape.

Figure 11.- Experimental and theoretical pressure distributions for the Newtonian- and integral-relation-derived tension-shell shapes for $Z = 0.65$, $r_n/r_b = 0.20$, $M_\infty = 3.0$, and $\alpha = 0$.

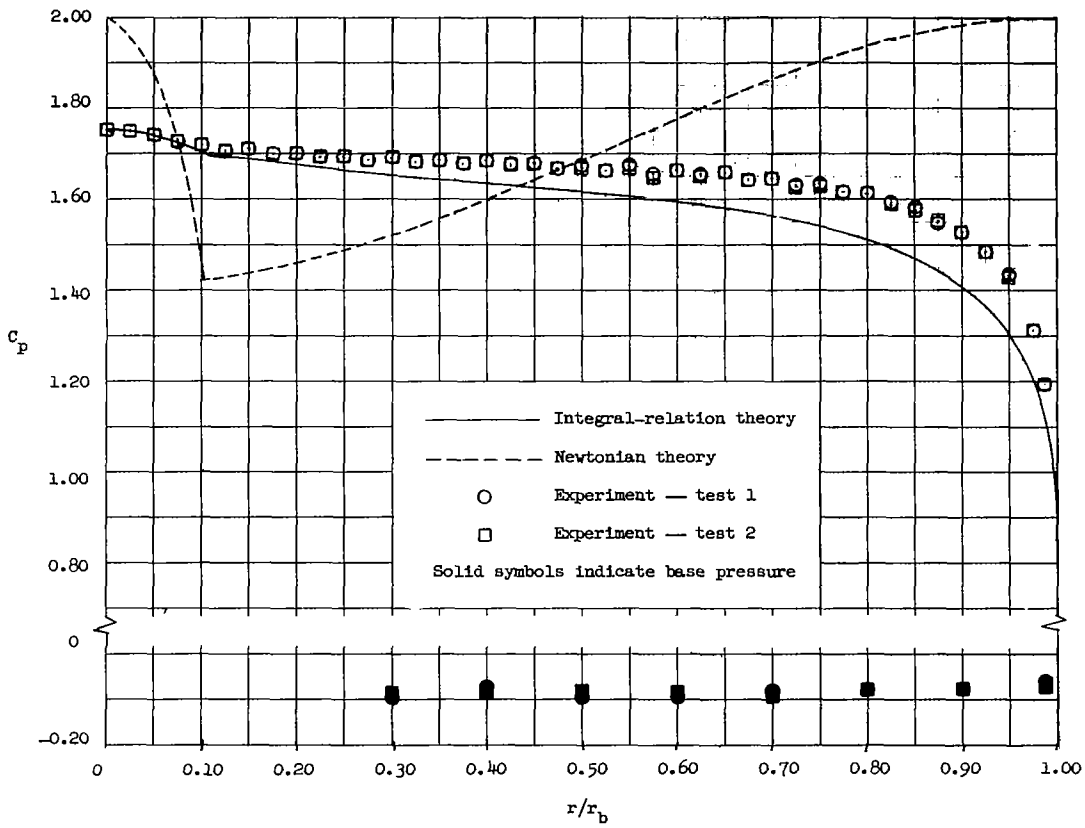

(b) Integral-relation-derived shape.

Figure 11.- Concluded.

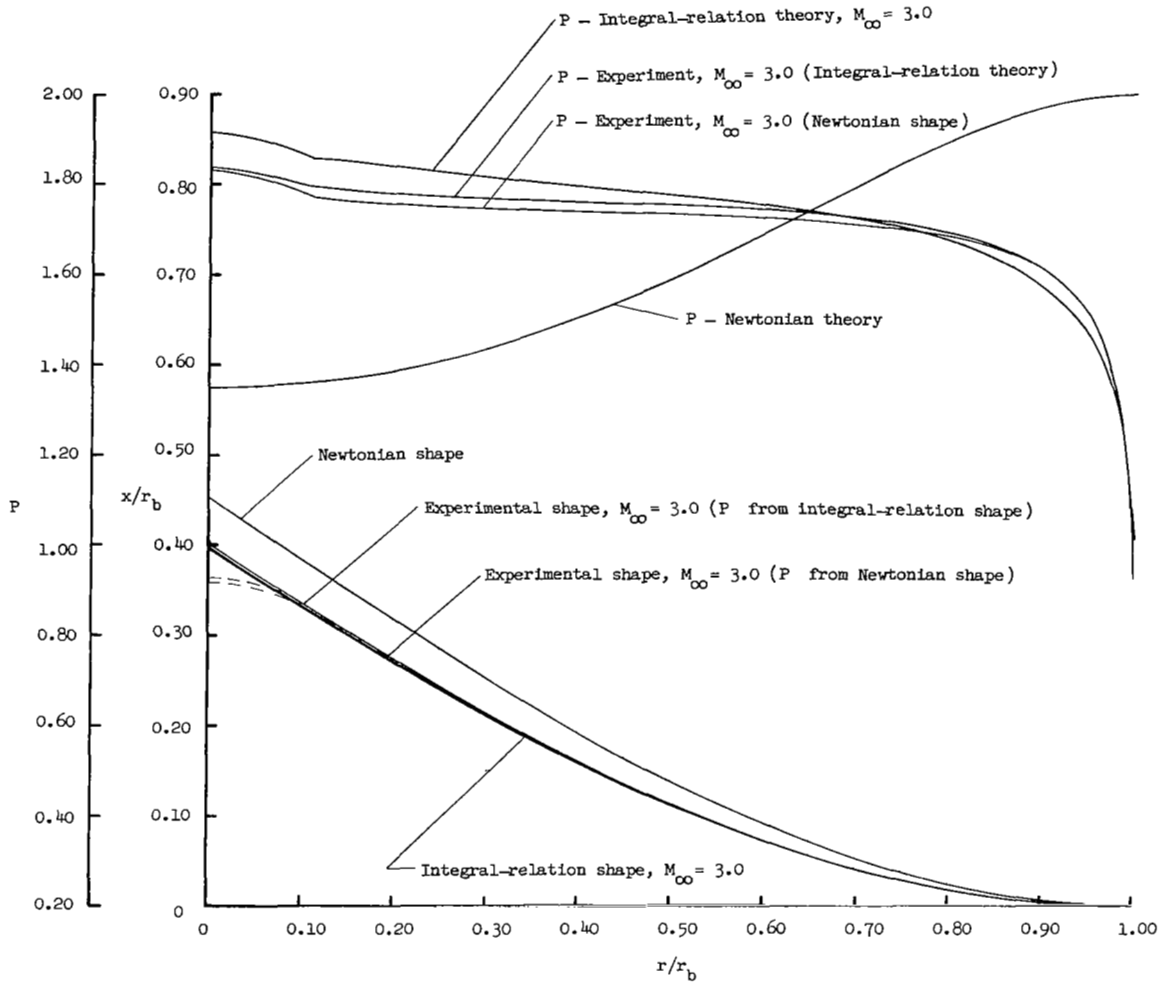

Figure 12.- Comparison of the Newtonian-derived, integral-relation-derived, and experimentally derived tension-shell shapes and pressure distributions for $Z = 0.65$ and $\alpha = 0$.

NASA-Langley, 1970 —— 1 L-6743